Non-linear Modelling and Verification of a Heaving Point Absorber for Wave Energy Conversion

Bingyong Guo, Ron Patton, *Life Fellow, IEEE,* Siya Jin, James Gilbert and Dan Parsons

Abstract—Although the heaving Point Absorber (PA) concept is well known in wave energy conversion research, few studies focus on appropriate modelling of non-linear fluid viscous and mechanical friction dynamics. Even though these concepts are known to have non-linear effects on the hydrodynamic system, most research studies consider linearity as a starting point and in so doing have a weak approach to modelling the true dynamic behaviour, particularly close to resonance. The sole use of linear modelling leads to limited ability to develop control strategies capable of true power capture optimisation and suitable device operation. Based on a 1/50 scale cylindrical heaving PA, this research focuses on a strategy for hydrodynamic model development and experimental verification. In this study, non-linear dynamics are considered, including the lumped effect of the fluid viscous and mechanical friction forces. The excellent correspondence between the derived non-linear model and wave tank tested PA behaviours provides a strong background for wave energy tuning and control system design.

Index Terms—point absorber modelling, non-linear hydrodynamics, wave tank tests, wave energy conversion.

NOMENCLATURE

Acc	Accelerometer.
BEM	Boundary element method.
LVDT	Linear variable displacement transducer.
NMSE	Normalised mean square-error.
NSEM	Navier-Stokes equation method.
PA	Point absorber.
PAWEC	Point absorber wave energy convertor.
PS,WG	Pressure sensor and wave gauge.
$A(\omega), A_\infty$	Added mass and its infinite frequency value.
$B(\omega)$	Radiation damping coefficient.
E_m	Normalised modelling error of f_{ln}.
f_c, F_c	Coulomb friction force and its coefficient.
f_s, F_s, C_s	Stribeck friction force and its coefficients.
f_d, C_f	Damping friction force and its coefficient.
f_f	Friction force $f_f = f_c + f_s + f_d$.
f_v, C_d	Fluid viscous force and its coefficient.
f_{ln}	Lumped non-linear force $f_{ln} = f_f + f_v$.
f_e, f_{hs}	Excitation and hydrostatic forces.
f_r, f_r'	Radiation force and its convolution term.
G_f	Goodness of fit of the radiation kernel function.
G_m	Goodness of matching for free-decay tests.
M, r, h, d	Buoy mass, radius, height and draught.

B. Guo, R. Patton, S. Jin and J. Gilbert are with the School of Engineering and Computer Science, University of Hull, Cottingham Road, Hull, UK, HU6 7RX (e-mail: B.Guo@2013.hull.ac.uk; R.J.Patton@hull.ac.uk; S.Jin@2015.hull.ac.uk; J.M.Gilbert@hull.ac.uk).

D. Parsons is with the School of Environmental Sciences, University of Hull, Cottingham Road, Hull, UK, HU6 7RX (e-mail: D.Parsons@hull.ac.uk).

I. INTRODUCTION

WITH the emergence of fossil fuel crisis, global attention on climate change and rising levels of the carbon dioxide emissions, renewable energy has been becoming an important research area and researchers have been turning to the value of harvesting energy from sea waves using Wave Energy Convertor (WEC) systems. Various WEC technologies and devices are reviewed in [1]–[5] and can be classified into five predominant types: (i) oscillating wave columns, e.g. the Mighty Whale, LIMPET; (ii) attenuator systems, e.g. Pelamis, the McCabe Wave Pump; (iii) Point Absorbers (PAs), e.g. the Archimedes Wave Swing, Wavebob; (iv) terminator devices, e.g. the Salter Duck, Oyster; (v) over-topping devices, e.g. TAPCHAN, the Wave Dragon.

Among the WECs currently being developed, a heaving PA is one of the simplest and most promising concepts [6], probably due to its favourable properties: ease of installation, economic operation, reliable survivability. The heaving PA can also be feasibly extended to form arrays and wave farms. For the Point Absorber Wave Energy Convertors (PAWECs), four kinds of modelling methods are widely applied in the problem of hydrodynamic prediction, as discussed in [7]: (i) analytical approaches, (ii) Boundary Element Methods (BEMs), (iii) BEMs superposed on non-linear forces methods (including the non-linear viscous, hydrostatic and Froude-Krylov forces and etc.) and (iv) Navier-Stokes Equation Methods (NSEMs).

The analytical approaches and BEMs provide linear prediction of the PAWEC hydrodynamics without considering any non-linear dissipative forces. One main drawback of these linear methods is that ignoring the dissipative forces always exaggerates the PAWEC motion and power production, especially when resonance is achieved via optimal control. If non-linear dissipative forces are superimposed on the BEMs, these approaches can provide more accurate PAWEC motion prediction. The NSEMs are fully non-linear methods which provide precise prediction of WEC hydrodynamics, especially in extreme wave conditions. However, the NSEMs are expensive in computation and their results are not straightforward for control system design. The BEMs superposed on non-linear fluid viscous and mechanical friction forces are evaluated in this study to provide more accurate PAWEC motion prediction.

Non-linear effects of fluid viscosity, end-protection and hydraulic Power Take-Off (PTO) system are studied in [8]. These non-linear effects are superimposed on a linear PAWEC model to evaluate phase control performance. The mechanical friction force is modelled as a pure damper in [8]. The importance of
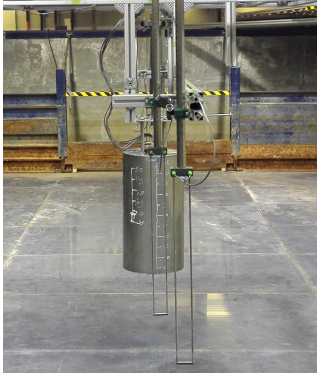
Fig. 1. A 1/50 PAWEC prototype installed for wave tank tests.

non-linear fluid viscous force is outlined experimentally in [9], [10]. For numerical modelling, the viscous force is linearised as an equivalent damper in [9], [10]. In this work, a non-linear PAWEC model is derived and validated considering the non-linear effects of both the fluid viscosity and mechanical friction. The fluid viscous force is modelled as the drag term in the Morison equation [11] with a semi-empirical viscous coefficient discussed in [12], [13]. The Tustin model [14] is used to represent the mechanical friction force for the PAWEC shown in Fig. 1. The fluid viscous and mechanical friction forces cannot be decoupled and in this work their summation is defined as a lumped non-linear force. Via the comparison between the numerical and experimental data, the mechanism by which these non-linear effects influence PAWEC motion and power dissipation is detailed in this work.

A 1/50 scale cylindrical heaving buoy (see Fig. 1) has been designed and constructed for wave tank tests, model verification and control system design. A wide variety of wave tank tests are conducted to validate the proposed lumped non-linear force model and the derived non-linear PAWEC model. The numerical results of the proposed models show a high accordance with the experimental data of wave tank tests.

The paper is structured as follows. In Section II, the wave-buoy interaction is studied to derive linear and non-linear models to represent the PAWEC dynamics. Section III describes the wave tank structure and the experimental configuration. Numerical results of the proposed models are compared with the experimental data in Section IV. Essential remarks and a concluding discussion are drawn up in Section V.

II. NUMERICAL MODELLING OF PA HYDRODYNAMICS

The hydrodynamics of the 1/50 scale heaving PAWEC are described in this Section. A linear model is derived to represent the buoy motion as a starting point with the radiation force approximated by a third order system, detailed in Section II-B. A non-linear model is proposed in Section II-C by considering the fluid viscous and mechanical friction forces.

A. Heaving Point Absorber Hydrodynamics

For a heaving cylindrical buoy excited by incident waves, the motion obeys Newton's second law [15], given as:

$$M\ddot{z}(t) = f_e(t) + f_r(t) + f_{hs}(t) + f_f(t) + f_v(t) + f_{pto}(t), \quad (1)$$

where $f_e(t)$ is the excitation force due to the incident wave; $f_r(t)$ is the radiation force related to the buoy velocity; $f_{hs}(t)$ is the hydrostatic force to represent the mismatch between the buoyancy and the gravity. $f_f(t)$ and $f_v(t)$ are the unavoidable mechanical friction and fluid viscous forces, respectively. $f_{pto}(t)$ represents the PTO force. M is the buoy mass and $z(t)$ is the PAWEC heaving displacement with the positive direction defined as upward in heave motion. For simplicity, only the heave motion is investigated in this paper and the PTO force is not considered since this paper focuses on the buoy hydrodynamics.

B. Linear Modelling of Heaving Point Absorber

1) Linear Hydrodynamics of Heaving Point Absorber: Based on the assumptions of (i) ideal fluid (inviscid, incompressible and irrotational), (ii) linear wave theory (Airy's wave theory) and (iii) small body motion [15], [16], Newton's second law in Eq. (1) can be rewritten as:

$$M\ddot{z}(t) = f_e(t) + f_r(t) + f_{hs}(t) + f_{ld}(t), \quad (2)$$

where $f_{ld}(t)$ represents the linear dissipative force considered as a combination of the linear mechanical friction [8] and the equivalent linearised fluid viscous force [9], [10]. Thus the linear dissipative force can be represented as:

$$f_{ld}(t) = -C_{ld}\dot{z}(t), \quad (3)$$

where C_{ld} is the equivalent linearised damping coefficient which can be determined via wave tank tests.

For a vertical cylinder, the hydrostatic force $f_{hs}(t)$ is proportional to the displacement $z(t)$, as:

$$f_{hs}(t) = -\rho g \pi r^2 z(t) = -K_{hs} z(t), \quad (4)$$

where $\rho = 1000 \mathrm{kgm}^{-3}$, $g = 9.81 \mathrm{ms}^{-2}$ are the water density and gravity constant, respectively. r and $K_{hs} = \rho g \pi r^2$ represent the buoy radius and hydrostatic stiffness, respectively.

The excitation force $f_e(t)$ is viewed as the system input and can be computed according to its analytical representations in [17], [18]. The radiation force $f_r(t)$ can be written in the time-domain, according to the Cummins equation [19]:

$$f_r(t) = -A_\infty \ddot{z}(t) - k_r(t) * \dot{z}(t), \quad (5)$$

where $A_\infty = 6.58 \mathrm{kg}$ is the added mass at infinite frequency and $k_r(t)$ is the Impulse Response Function (IRF) of the radiation force, also known as the kernel function. $X * Y$ represents the convolution operation between X and Y. Alternatively, the radiation force can be written in the frequency-domain as:

$$F_r(j\omega) = (\omega^2 A(\omega) - j\omega B(\omega))Z(j\omega), \quad (6)$$

where ω is the angular frequency. $F_r(j\omega)$, $A(\omega)$, $B(\omega)$ and $Z(j\omega)$ are the frequency-domain representations of the radiation force, added mass, radiation damping and buoy displacement, respectively. The relationship between the time- and frequency-domain coefficients is derived in [20] and referred to as the Ogilvie relation, given as:

$$A(\omega) = A_\infty - \frac{1}{\omega}\int_0^\infty k_r(t)sin(\omega t)dt, \quad (7)$$

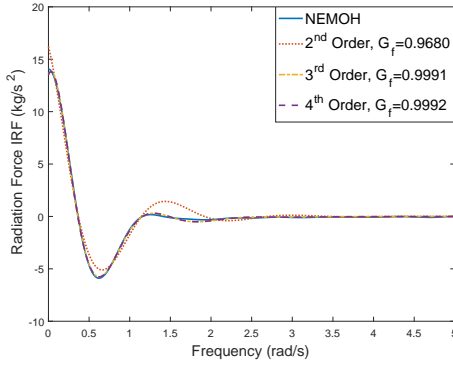$$B(\omega) = \int_0^\infty k_r(t)cos(\omega t)dt. \quad (8)$$

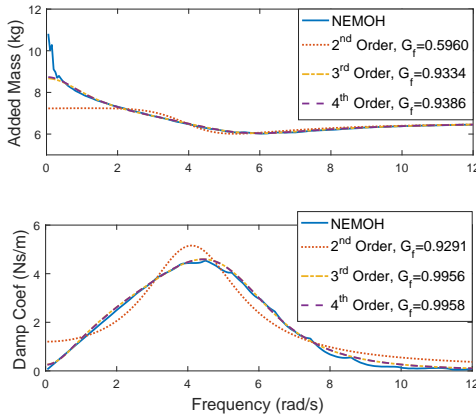Fig. 2. IRFs of NEMOH results and the identified systems.

Fig. 3. Radiation coefficients of NEMOH results and the identified systems.

The hydrodynamic coefficients are obtained by solving a boundary value problem in the BEM code NEMOH [21]. It provides an alternative to commercial BEM packages, like WAMIT$^{\circledR}$ and AQWA$^{\text{TM}}$. The simulation in NEMOH is based on the $1/50$ scale PAWEC in Fig. 1, which is a semi-submerged buoy with a radius $r = 0.15$m, a draught $d = 0.28$m and a mass $M = 19.79$kg. The time-domain radiation force IRF is shown in Fig. 2 and Fig. 3 illustrates the frequency-domain added mass and radiation damping coefficient. The convolution operation associated with the radiation force in Eq. (5) is inconvenient for buoy hydrodynamic analysis and control system design. Hence, it is important to approximate the convolution term with a finite order system.

2) Finite Order Approximation of Radiation Force: For control system design, time-domain models are preferred. Finite order approximations of the radiation force are proposed for offshore structure motion prediction in [22], [23]. For PAWEC system analysis, it is common to approximate this convolution term by a finite order transfer function or state-space model using system identification methods [24], [25]. The radiation force causality is proved in [26]. In this work, the realisation theory is applied to deduce a linear state-space model from the radiation force IRF.

The convolution term is defined as a subsystem $f'_r(t)$ as:

$$f'_r(t) = k_r(t) * \dot{z}(t) = \int_0^t k_r(t - \tau)\dot{z}(\tau)d\tau. \qquad (9)$$

The IRF $k_r(t)$ in Eq. (9) is obtained from NEMOH and shown in Fig. 2. The realisation theory is applied to deduce a linear state-space model directly with MATLAB$^{\circledR}$ function *imp2ss* [27] from the *Robust Control Toolbox*. Thus the convolution term can be approximated as:

$$\dot{x}_r(t) = A_r x_r(t) + B_r \dot{z}(t), \qquad (10)$$
$$f'_r(t) \approx C_r x_r(t), \qquad (11)$$

where $x_r(t) \in \mathbb{R}^{n \times 1}$ is the state vector for the identified system and n is the system order. $\dot{z}(t)$ is the buoy velocity. $A_r \in \mathbb{R}^{n \times n}$, $B_r \in \mathbb{R}^{n \times 1}$, $C_r \in \mathbb{R}^{1 \times n}$ are the system matrices.

The order of the initially identified system is quite high and model reduction is required and achieved by the square-root balanced model reduction method with MATLAB$^{\circledR}$ function *balmar* [28]. To determine the system order n, a goodness of fit G_f is defined with a cost-function of the Normalised Mean Square-Error (NMSE), as:

$$G_f = 1 - \left\| \frac{k_r(t) - k_{r,i}(t)}{k_r(t) - \bar{k}_r(t)} \right\|_2^2, \qquad (12)$$

where $\|X\|_2$ is the 2-norm operation of X; $\bar{k}_r(t)$ is the mean value of $k_r(t)$; $k_{r,i}(t)$ is the identified IRF. G_f tends to 1 for close model-data matching and tends to $-\infty$ for poor model-data matching.

The IRFs of the second, third and fourth order identified systems are compared with the original IRF from NEMOH in Fig. 2. The values of G_f are 0.9680, 0.9991 and 0.9992 for the second, third and fourth order systems, respectively. The third order system IRF matches the original IRF well and a further increase of system order introduces extra system complexity without further improvement of the approximation accuracy.

A simple validation of the time-domain IRF identification technique can be achieved by checking the frequency-domain radiation coefficients. According to the Ogilvie relation [20], the added mass and radiation damping coefficient of the identified systems can be computed according to Eqs. (7) and (8), which are compared with the NEMOH results in Fig. 3. The second order system cannot represent the radiation coefficients accurately at low wave frequencies, especially for $\omega \leq 5$rad/s. The third and fourth order systems approximate the NEMOH results with a high goodness of fit, both in the time- and frequency-domains.

Therefore, $n = 3$ is selected and a third order state-space model is adopted to replace the convolution term in Eq. (5) to provide a straightforward and convenient representation for the PAWEC numerical modelling and control system design. The system matrices of Eqs. (10) and (11) are given as:

$$A_r = \begin{bmatrix} -3.1848 & -4.3372 & -3.1009 \\ 4.3372 & -0.0875 & -0.3882 \\ 3.1009 & -0.3882 & -2.8499 \end{bmatrix}, \qquad (13)$$
$$B_r = \begin{bmatrix} -40.6964 & 5.9737 & 16.2722 \end{bmatrix}^\top, \qquad (14)$$
$$C_r = \begin{bmatrix} -0.4070 & -0.0597 & -0.1627 \end{bmatrix}. \qquad (15)$$

3) A Linear Model of Heaving Point Absorber: According to Eq. (2), if the wave excitation force is viewed as the input and the buoy displacement is set as the output, a linear model from the wave excitation force to the buoy motion, referred to as the *force-to-motion* model, is written as:

$$x(t) = \begin{bmatrix} x_r(t) & z(t) & \dot{z}(t) \end{bmatrix}^\top, \quad (16)$$
$$\dot{x}(t) = Ax(t) + Bf_e(t), \quad (17)$$
$$z(t) = Cx(t), \quad (18)$$

with

$$A = \begin{bmatrix} A_r & 0 & B_r \\ 0 & 0 & 1 \\ -\frac{C_r}{M+A_\infty} & -\frac{K_{hs}}{M+A_\infty} & -\frac{C_{ld}}{M+A_\infty} \end{bmatrix}, \quad (19)$$

$$B = \begin{bmatrix} 0 & 0 & 0 & 0 & 1/(M+A_\infty) \end{bmatrix}^\top, \quad (20)$$

$$C = \begin{bmatrix} 0 & 0 & 0 & 1 & 0 \end{bmatrix}. \quad (21)$$

If a non-zero initial condition $x(0)$ and an excitation force $f_e(t) \equiv 0$N are applied to excite the linear model at time $t = 0$s, the system response is called the zero-input response, identified here as the *free-decay test*, written as:

$$z(t) = Ce^{At}x(0). \quad (22)$$

C. Non-linear Modelling of Heaving Point Absorber

For most offshore structures, the linear assumptions can be satisfied and thus the linear modelling approach can provide accurate hydrodynamic prediction. However, the PAWEC motion can be very large when the resonance is achieved by optimal control strategies. In this situation, the relative velocity between the PAWEC and the water around it is large and thus the fluid viscous force cannot be ignored. For the 1/50 PAWEC, the mechanical friction force is not negligible compared with the wave conditions during tank tests. In this work, the quadratic fluid viscous force is modelled as the drag force term in the Morison equation [11]. Whilst, the mechanical friction force is modelled as a combination of the Coulomb, Stribeck, and damping forces [14]. The summation of the fluid viscous and mechanical friction forces is defined as the lumped non-linear force and is the focus of this Section, leading to a more applicable non-linear PAWEC model.

1) Modelling of Fluid Viscous Force: As suggested in [7], [8], [29], the viscous force $f_v(t, x)$ follows the drag term in the Morison equation [11], given as:

$$f_v(t,x) = -0.5\rho C_d \pi r^2 (\dot{z}(t) - u(t))|\dot{z}(t) - u(t)|, \quad (23)$$

where C_d is the viscous coefficient; $u(t)$ is the vertical velocity of water particles around the buoy. C_d is a function of the Keulegan-Carpenter number K_c, the Reynolds number R_e and the roughness number K_r [12]. As suggested in [12], the empirical value of C_d varies from 0.6 to 1.2. For small K_c ($K_c \approx 3.67$ for the 1/50 PA), the appropriate range of C_d from 0.8 to 1 is commonly acceptable [13]. In this study, C_d is evaluated experimentally in Section III-C.
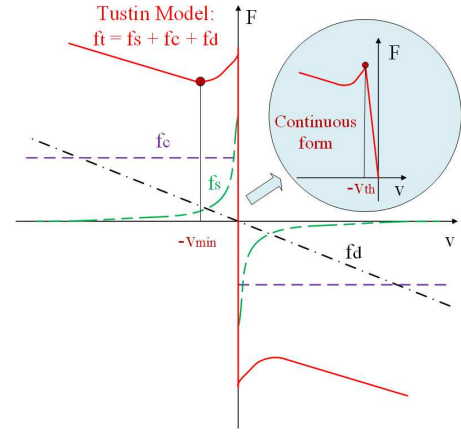

Fig. 4. Sketch of the Tustin model with continuous approximation (inset).

2) Modelling of Mechanical Friction: Several mechanical friction models are reviewed in [30]. Among these, the Tustin model is expressed as the combination of the Coulomb, Stribeck and damping forces in [14], [30]–[32]. As shown in Fig. 4, the friction force components can be expressed as:

$$f_c(t,x) = -s_v F_c, \quad (24)$$
$$f_s(t,x) = -s_v F_s e^{-C_s|\dot{z}(t)|}, \quad (25)$$
$$f_d(t,x) = -s_v C_f |\dot{z}(t)|, \quad (26)$$

where $s_v = sgn(\dot{z}(t))$ is the sign of the buoy velocity; $f_c(t)$ is the Coulomb friction force with its coefficient F_c; $f_s(t)$ is the Stribeck friction force with its coefficient F_s and shape factor C_s; $f_d(t)$ is the damping friction force with its coefficient C_f. The negative symbol means that the friction force always impedes the PAWEC velocity.

As shown in Fig. 4, the Tustin model is expressed as:

$$f_f(t,x) = -s_v(F_c + F_s e^{-C_s|\dot{z}(t)|} + C_f|\dot{z}(t)|). \quad (27)$$

The Stribeck shape factor can be determined by the velocity V_{min} which corresponds to the minimum friction in Fig. 4, given as:

$$C_f - F_s C_s e^{-C_s V_{min}} = 0. \quad (28)$$

In this study, V_{min}, C_f and F_s are determined experimentally and thus C_s is obtained by solving Eq. (28).

A key characteristic of this model is that the friction is discontinuous at the zero-velocity point. The discontinuity may cause difficulties for numerical modelling of the friction force. The mechanical friction force can be estimated from the velocity measurement made during wave tank tests. Measurement noise is unavoidable and has a significant influence on the friction modelling, especially when the velocity is close to zero. Therefore, a velocity threshold V_{th} is applied to the Tustin model in this work to improve its continuity within the zero-velocity region. As shown in the inset in Fig. 4, the continuous formulation of the Tustin model can be rewritten as:

$$f_f(t,x) = \begin{cases} -s_v(F_c + F_s e^{-C_s|\dot{z}|} + C_f|\dot{z}|), & |\dot{z}| \geq V_{th}; \\ -s_v(F_c + F_s e^{-C_s V_{th}} + C_f V_{th})\frac{|\dot{z}|}{V_{th}}, & |\dot{z}| < V_{th}. \end{cases} \quad (29)$$
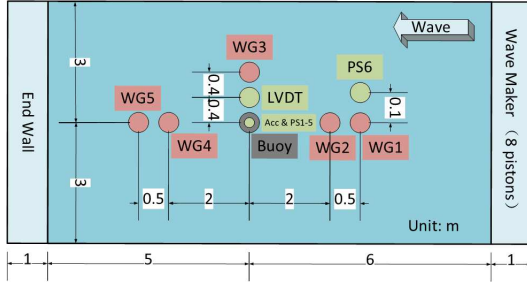
Fig. 5. Sketch of the wave tank and the device installation.

Fig. 6. Free-fall tests to determine the Coulomb and damping coefficients.

V_{th} is always set with a very small value. In the friction model in Eq. (29), there are five unknown parameters (F_s, F_c, C_f, V_{th} and V_{min}) to be determined experimentally.

3) A Non-linear PAWEC Model: During wave tank tests, the fluid viscous and mechanical friction forces are lumped and cannot be decoupled from each other. Therefore, a lumped non-linear force $f_{ln}(t, x)$ is defined as the summation of $f_v(t, x)$ and $f_f(t, x)$, given as:

$$f_{ln}(t, x) = f_v(t, x) + f_f(t, x). \tag{30}$$

Substituting Eq. (30) into Eq. (1) gives:

$$M\ddot{z}(t) = f_e(t) + f_r(t) + f_{hs}(t) + f_{ln}(t, x). \tag{31}$$

Thus the buoy dynamics can be expressed as a non-linear model in a state-space formulation as:

$$\dot{x}(t) = Ax(t) + Bf_e(t) + Bf_{ln}(t, x), \tag{32}$$
$$z(t) = Cx(t). \tag{33}$$

III. FLUME TESTS AND MODEL VERIFICATION

For model validation, a variety of free-fall and free-decay tests are conducted in a wave tank. This Section details the experimental configuration, the free-fall and free-decay tests.

A. Experimental Configuration

As shown in Fig. 5, the wave tank is 13m in length, 6m in width and 2m in height (water depth 0.9m). Up to 8 pistons can be selected to generate regular/irregular waves.

The $1/50$ scale buoy is installed in the centred area of the wave tank. Five Wave Gauges (WGs) are mounted to measure the water elevation in real-time. Five Pressure Sensors (PS1-5) are installed at the PAWEC base to measure the dynamic pressure acting on the hull. To investigate the buoy motion, a Linear Variable Displacement Transducer (LVDT) is connected to the buoy rigidly to record the displacement and a 3-axis Accelerometer (Acc) is mounted at the top of the buoy to measure the buoy heaving acceleration. All the sensing signals are collected via a 16-bit data acquisition system (USB-6210) connected with LABVIEW$^{\text{TM}}$. The sampling frequency is 100Hz.
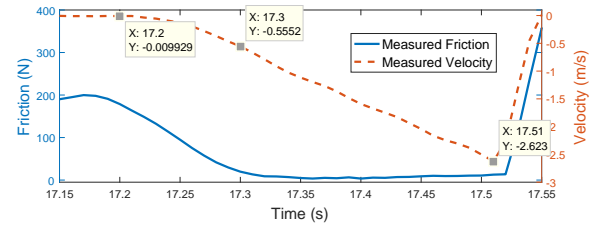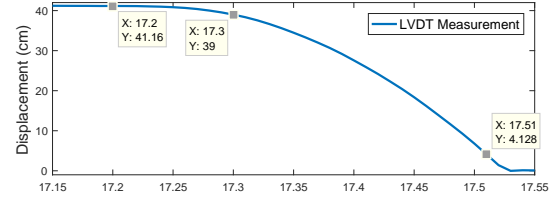
B. Free-fall Tests

The mechanical friction profile can be estimated experimentally. In *free-fall tests*, the buoy is lifted into the air (above the water), held stable for a short period and then released suddenly. The free-fall motion fits Newton's second law and hence the mechanical friction force can be "pseudo" measured as $f_{f,m}(t)$, written as:

$$f_{f,m}(t) = -Mg - Ma_m(t), \tag{34}$$

where $a_m(t)$ is the measured heaving acceleration. Meanwhile, the LVDT records the buoy displacement to provide "pseudo" velocity measurement $v_m(t)$ via the difference method.

The free-fall test results are shown in Fig. 6. According to the displacement and velocity measurements, the buoy is released at $t = 17.20$s and then experiences free acceleration until $t = 17.51$s, within which the measured velocity increases stably. After $t = 17.51$s, the buoy hits the wave tank gantry.

The parameters of the Coulomb and damping forces in Eq. (29) are obtained via linear least-squares fitting applied to the measured friction and velocity data within the time interval from $t = 17.30$s to $t = 17.51$s. The resulting parameters are:

$$f_{f,m}(t) = F_c - C_f v_m(t) = 2.6579 - 2.988 v_m(t). \tag{35}$$

Thus $F_c = 2.6579$N and $C_f = 2.988$Nsm^{-1} are chosen for the mechanical friction model.

C. Free-decay Tests

As defined in Eq. (22), free-decay tests are conducted in the wave tank. The buoy is pushed down to a non-zero initial position, held stable for a short term and then released. During free-decay tests, the lumped non-linear force is "pseudo" measured as $f_{ln,m}(t)$, given as:

$$f_{ln,m}(t) = Ma_m(t) - \pi r^2 \bar{p}(t), \tag{36}$$

where $\bar{p}(t)$ is the mean value of PS1-5 measurements. The pressure is not evenly distributed on the wet surface of the buoy and thus $\pi r^2 \bar{p}$ in Eq. (36) only gives a simple approximation of the wave-buoy interaction.
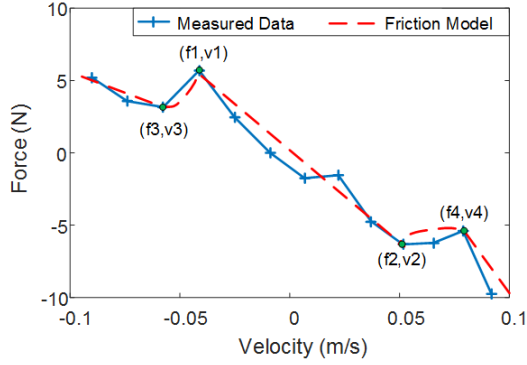
Fig. 7. Zero-crossing point to determine the Stribeck force parameters.

Fig. 8. Comparison of power dissipation between the viscous, Coulomb, Stribeck and damping forces.

During a free-decay test, the buoy oscillates several times and is damped to its equilibrium point. The point where $v_m(t)$ changes its direction is defined as the *zero-crossing point*. Within the zero-crossing point vicinity, the measured velocity is close to zero and hence the fluid viscous force is small enough to be ignored. Therefore the friction parameters in Eq. (29), F_s and V_{min}, can be observed from the measurements of $f_{ln,m}(t)$ and $v_m(t)$. According to the comparison between the experimental data and the Tustin model in Fig. 7, the parameters F_s, V_{th} and V_{min} are written as:

$$F_s = |f_1 - f_2|/2 - F_c, \tag{37}$$
$$V_{th} = |v_2 - v_1|/2, \tag{38}$$
$$V_{min} = |v_4 - v_3|/2, \tag{39}$$

where f_1, f_2, v_1, v_2, v_3 and v_4 correspond to the experimental data shown in Fig. 7. The average values of $F_s = 3.5574$N, $V_{th} = 0.0398 \text{ms}^{-1}$ and $V_{min} = 0.0838 \text{ms}^{-1}$ are computed from ten zero-crossing points leading to the data in Table I (see Section IV-B). Solving Eq. (28) then gives $C_s = 48.37 \text{sm}^{-1}$.

Since the friction model is determined, the viscous coefficient C_d is the only unknown parameter in the non-linear PAWEC model expressed in Eqs. (32) and (33). To estimate C_d from the free-decay tests, the non-linear least-squares data fitting method is applied to minimise the displacement error between numerical and experimental data, given as:

$$C_d = \min_{C_d} \|d_{tt} - d_{nm}(C_d)\|_2^2, \tag{40}$$

where d_{tt} and d_{nm} are the normalised tank test displacement and the corresponding non-linear model simulation. For ten free-decay tests with initial displacements from $z_i = -2$cm to $z_i = -20$cm, the average value of the viscous coefficient is $C_d = 0.9382$.

IV. RESULTS COMPARISON AND DISCUSSION

In this Section, the modelled and tested lumped non-linear force results are compared in Section IV-A. Further comparison is made by the normalised displacement responses between free-decay tests and the linear/non-linear modelling in Section IV-B. The comparison emphasises the importance of the non-linear fluid viscous and mechanical friction forces and the way in which they influence the PAWEC dynamics.
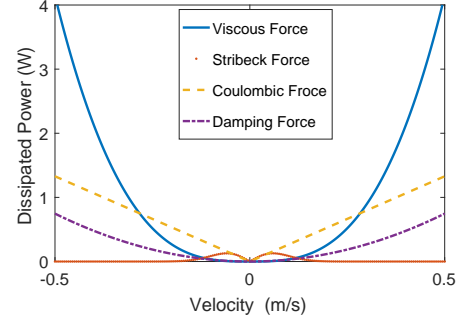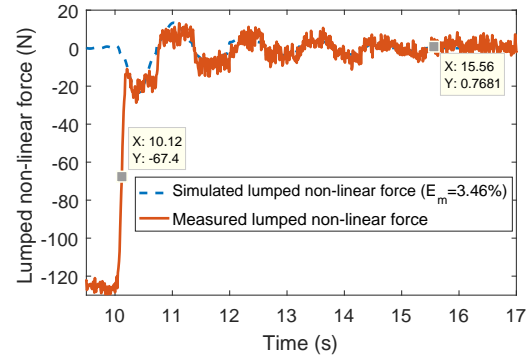

Fig. 9. Comparison of the measured and simulated lumped non-linear forces.

A. Model Verification of Lumped Non-linear Force

The power dissipated by the mechanical friction can be decomposed according to the friction components, as:

$$P_c(t) = |f_c(t)\dot{z}(t)| = F_c|\dot{z}(t)|, \tag{41}$$
$$P_s(t) = |f_s(t)\dot{z}(t)| = F_s e^{-C_s|\dot{z}(t)|}|\dot{z}(t)|, \tag{42}$$
$$P_d(t) = |f_d(t)\dot{z}(t)| = C_f|\dot{z}(t)|^2, \tag{43}$$

where $P_c(t)$, $P_s(t)$ and $P_d(t)$ represent the dissipated power by the Coulomb, Stribeck and damping forces, respectively.

In free-decay tests, the velocity of water particles is small enough to be ignored and hence Eq. (23) can be rewritten as:

$$f_v(t) = -0.5\rho C_d \pi r^2 \dot{z}(t)|\dot{z}(t)|. \tag{44}$$

Thus the associated power dissipation $P_v(t)$ is given as:

$$P_v(t) = |f_v(t)\dot{z}(t)| = 0.5\rho C_d \pi r^2 |\dot{z}(t)|^3. \tag{45}$$

The comparison between these power dissipations are shown in Fig. 8. According to Fig. 8, the fluid viscous and Coulomb forces are important since they dissipate significant power. The damping friction force does not consume as much power as the fluid viscous and Coulomb forces but cannot be neglected when the velocity is large. When the velocity decays to a small amount, the Stribeck force is an important factor that impedes the buoy motion back on returning to the equilibrium point. Therefore, the lumped non-linear force is modelled as a combination of the fluid viscous, Coulomb, Stribeck and damping forces in Eq. (30).

TABLE I
NORMALISED MODELLING ERROR/GOODNESS OF THE LUMPED
NON-LINEAR FORCE/NON-LINEAR MODEL.

Initial Position	E_m Eq. (48)	G_m Eq. (49)	Initial Position	E_m Eq. (48)	G_m Eq. (49)
-2cm	1.40%	0.9540	-12cm	3.41%	0.9614
-4cm	1.61%	0.9713	-14cm	3.72%	0.9704
-6cm	4.63%	0.9697	-16cm	2.33%	0.9805
-8cm	4.84%	0.9869	-18cm	3.46%	0.9839
-10cm	1.73%	0.9841	-20cm	1.67%	0.9685

Fig. 10. Comparison of normalised displacement between numerical and experimental results.

For a free-decay test with initial position -18cm, the measured and simulated results of the lumped non-linear force are shown in Fig. 9. The buoy is released at time $t_r = 10.12$ s (defined as the *releasing time t_r*) and is damped to its equilibrium point at time $t_s = 15.56$ s (defined as the *settling time t_s*). The simulation results of the lumped non-linear force fit the experimental measurements to a high degree (with a normalised modelling error $E_m = 3.46\%$).

E_m is defined as the *normalised modelling error* of the lumped non-linear force by means of the average dissipated power from the releasing time t_r to the settling time t_s, as:

$$P_{ms} = \frac{\int_{t_r}^{t_s} v_m(t) f_{lnms}(t) dt}{t_s - t_r}, \tag{46}$$

$$P_{md} = \frac{\int_{t_r}^{t_s} v_m(t) f_{lnmd}(t) dt}{t_s - t_r}, \tag{47}$$

$$E_m = \left| \frac{P_{md} - P_{ms}}{P_{ms}} \right| \cdot 100\%, \tag{48}$$

where $f_{lnms}(t)$ is measured lumped non-linear force; $f_{lnmd}(t)$ is the modelled lumped non-linear force; P_{ms} and P_{md} are the average values of the measured and modelled power dissipations from t_r to t_s, respectively.

A wide range of free-decay tests are conducted to check the modelling accuracy of the lumped non-linear force. Table I shows that the mathematical model of the lumped non-linear force fits the experimental measurements with a very small error ($< 5\%$). Thus this lumped non-linear force model is accurate and useful for deriving a practical non-linear numerical solution for the buoy motion prediction.

B. Free-decay Test Results Comparison

For the free-decay tests with initial displacements of -3cm, -8cm and -18cm, the normalised displacement responses of the linear and non-linear models are compared with the experimental data and shown in Fig. 10. For the linear model in Eqs. (17) and (18), the equivalent linearised damping coefficient C_{ld} is optimised for the -8cm free-decay test and is determined as $C_{ld} = 21.50$Nsm^{-1}. The non-linear model considering the fluid viscous and mechanical friction forces is expressed in Eqs. (32) and (33). Fig. 10 indicates:

- The proposed linear model with equivalent linearised damping coefficient gives the same normalised displacement response for all free-decay tests regardless of initial
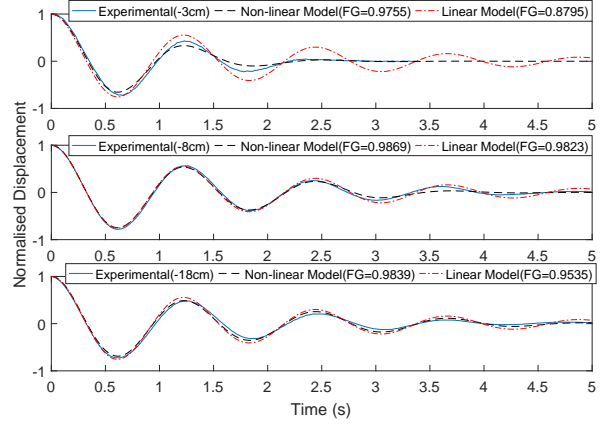
displacements. The linear model shows a high correspondence to the -8cm free-decay test, since C_{ld} is optimised at this initial condition. However, this linear model cannot fit the -3cm and -18cm free-decay tests. To gain a more accurate PAWEC motion prediction, the equivalent linearised damping coefficient should be optimised at each initial displacement of free-decay tests.

- Compared to the linear model, the non-linear model represented in Eqs. (32) and (33) fits the experimental data well with a wide range initial displacements. As shown in Fig. 10, the linear and non-linear models give almost the same results as the experimental data for the free-decay test initialised at -8cm. Furthermore, for the -3cm and -18cm free-decay tests, the non-linear model maintains a high correspondence to the experimental data, whilst the correspondence between the linear model simulations and the free-decay tests varies according to initial displacements. This is to be expected since the non-linear model in terms of the fluid viscous and Tustin friction corresponds closely with the non-linear behaviour of the experimental tank data, whilst the linearised model is only valid for small perturbations around the chosen displacement datum or equilibrium.

For the -3cm, -8cm and -18cm free-decay tests, the dissipated power defined in Eqs. (41), (42),(43) and (45) are compared in Fig. 11, which illustrates that:

- For the -3cm free-decay test, the Coulomb friction force dissipates most power. Only a small amount power is consumed by the Stribeck, damping and viscous forces.
- For the -8cm free-decay test, the Coulomb and fluid viscous forces consume the main part of power and the rest is dissipated by the damping friction force.
- For the -18cm free-decay test, the fluid viscous force uses most of power and the rest is dissipated by the Coulomb and damping friction forces. From the viewpoint of power dissipation, the influence of the Stribeck friction force can be ignored in this test.
- From the viewpoint of the normalised displacement response, the Stribeck friction force is important to damp
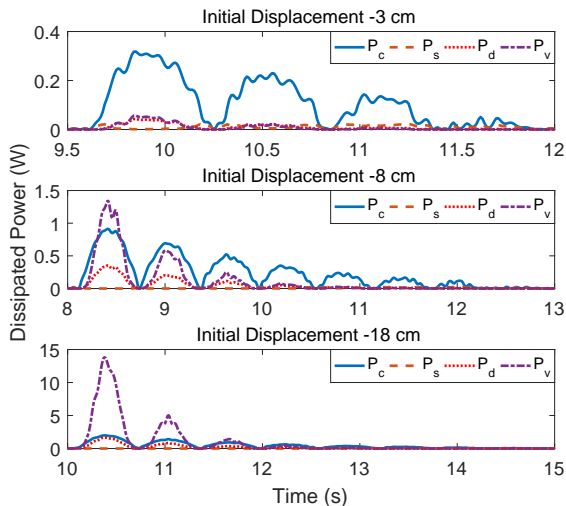
Fig. 11. Power dissipation comparison among the dissipative forces.

the buoy back to its equilibrium point when the velocity is small. This is illustrated by the -3cm free-decay test results and shown in Fig. 10.

The influence of the dissipative forces on the PAWEC dynamics are studied in terms of the normalized displacement response and power dissipation, shown in Figs. 10 and 11. To evaluate the model-data matching of the normalised displacement, a *goodness of matching* G_m is defined by the NMSE cost-function as:

$$G_m = 1 - \left\| \frac{d_{tt}(t) - d_{nm}(t)}{d_{tt}(t) - \bar{d}_{tt}(t)} \right\|_2^2, \qquad (49)$$

where $d_{tt}(t)$ and $d_{nm}(t)$ are the normalised tank test displacement and the corresponding non-linear model simulation.

The free-decay tests are conducted with a wide range of initial displacements from -2cm to -20cm. The goodness of matching of the non-linear model is shown in Table I. The non-linear model simulation results fit well with the free-decay tests, with a goodness of matching over 0.95. Therefore, it is concluded that the proposed non-linear model represents the $1/50$ scale prototype dynamics accurately for a wide range of free-decay tests.

V. CONCLUSION

A non-linear model is proposed to represent the PAWEC dynamics by considering the fluid viscous and mechanical friction forces. A $1/50$ scale heaving PAWEC prototype has been constructed for model verification and the non-linear model simulation results fit the experimental data to a high extent ($G_m > 0.95$). Thus Eqs. (32) and (33) provide a straightforward and accurate non-linear representation for the PAWEC dynamic modelling and control system design.

The non-linear influence of the Coulomb, Stribeck, damping and fluid viscous forces on the PAWEC dynamics is investigated in terms of normalised displacement response and power dissipation, shown in Figs. 10 and 11. For a wide variety of free-decay tests, the modelled lumped non-linear force fits the experimental data well and the normalised modelling error is within 5% (see Table I). Thus the proposed model of the lumped non-linear force in Eq. (30) can represent the non-linear phenomena of the $1/50$ prototype for free-decay tests. For the PAWEC oscillation under wave excitation, the validity of Eq. (30) needs more numerical and experimental study. It is understood that for the scaled system the mechanical friction effect can be proportionally greater than that for the full size PAWEC system. However, the effect of the non-linear fluid viscous force will still be significant in the full scale system for which this approach will still be of considerable value.

One main drawback of the proposed model is that the input is the wave excitation force rather than incident waves. The wave excitation force is actually unmeasurable whilst waves are measurable. Ongoing work focuses on the system identification of the wave excitation force to derive a non-linear wave-to-motion model of the PAWEC system. The parameters may drift over time and can thus be considered as an incipient fault effect either considered together or individually. An on-line machine learning technique together with fault tolerant control is to be used for drift compensation (by updating the PAWEC model).

REFERENCES

[1] A. d. O. Falcao, "Wave energy utilization: A review of the technologies," *Renew. Sust. Energ. Rev.*, vol. 14, no. 3, pp. 899–918, 2010.

[2] A. Babarit, J. Hals, M. Muliawan, A. Kurniawan, T. Moan, and J. Krokstad, "Numerical benchmarking study of a selection of wave energy converters," *Renew. Energ.*, vol. 41, pp. 44–63, 2012.

[3] B. Drew, A. Plummer, and M. N. Sahinkaya, "A review of wave energy converter technology," *P. I. Mech. Eng. A-J. Pow.*, vol. 223, no. 8, pp. 887–902, 2009.

[4] T. Thorpe, "An overview of wave energy technologies: status, performance and costs," *Wave power: moving towards commercial viability*, vol. 26, pp. 50–120, 1999.

[5] A. Clément, P. McCullen, A. Falcão, A. Fiorentino, F. Gardner, K. Hammarlund, G. Lemonis, T. Lewis, K. Nielsen, S. Petroncini *et al.*, "Wave energy in europe: current status and perspectives," *Renew. Sust. Energ. Rev.*, vol. 6, no. 5, pp. 405–431, 2002.

[6] P. Ricci, J. Lopez, M. Santos, J. Villate, P. Ruiz-Minguela, F. Salcedo, and A. d. O. Falcao, "Control strategies for a simple point-absorber connected to a hydraulic power take-off," in *Proc. EWTEC*, 2009, pp. 7–10.

[7] Y. Li and Y.-H. Yu, "A synthesis of numerical methods for modeling wave energy converter-point absorbers," *Renew. Sust. Energ. Rev.*, vol. 16, no. 6, pp. 4352–4364, 2012.

[8] H. Eidsmoen, "Simulation of a slack-moored heaving-buoy wave-energy converter with phase control," Division of Physics, NTNU, Trondheim, Norway, Tech. Rep., 1996.

[9] D. Son, V. Belissen, and R. W. Yeung, "Performance validation and optimization of a dual coaxial-cylinder ocean-wave energy extractor," *Renew. Energ.*, vol. 92, pp. 192–201, 2016.

[10] G. Bacelli, R. G. Coe, D. Patterson, and D. Wilson, "System identification of a heaving point absorber: Design of experiment and device modeling," *Energies*, vol. 10, no. 4, p. 472, 2017.

[11] J. Morison, J. Johnson, and S. Schaaf, "The force exerted by surface waves on piles," *J. Pet. Technol.*, vol. 2, no. 05, pp. 149–154, 1950.

[12] O. T. Gudmestad and G. Moe, "Hydrodynamic coefficients for calculation of hydrodynamic loads on offshore truss structures," *Mar. Struct.*, vol. 9, no. 8, pp. 745–758, 1996.

[13] T. Sarpkaya, "Force on a circular cylinder in viscous oscillatory flow at low keulegan–carpenter numbers," *J. Fluid Mech.*, vol. 165, pp. 61–71, 1986.

[14] A. Tustin, "The effects of backlash and of speed-dependent friction on the stability of closed-cycle control systems," *Journal of the Institution of Electrical Engineers-Part IIA: Automatic Regulators and Servo Mechanisms*, vol. 94, no. 1, pp. 143–151, 1947.

[15] J. Falnes, *Ocean waves and oscillating systems: linear interactions including wave-energy extraction*. Cambridge University Press, 2002.

[16] F. Fusco and J. V. Ringwood, "Hierarchical robust control of oscillating wave energy converters with uncertain dynamics," *IEEE Trans. Sust. Energ.*, vol. 5, no. 3, pp. 958–966, 2014.

[17] J. N. Newman, "The exciting forces on fixed bodies in waves," *Journal of Ship Research*, vol. 4, pp. 10–17, 1962.

[18] M. Greenhow and S. White, "Optimal heave motion of some axisymmetric wave energy devices in sinusoidal waves," *Appl. Ocean Res.*, vol. 19, no. 3-4, pp. 141–159, 1997.

[19] W. Cummins, "The impulse response function and ship motions," DTIC Document, Tech. Rep., 1962.

[20] T. F. Ogilvie, "Recent progress toward the understanding and prediction of ship motions," in *5th Symposium on naval hydrodynamics*, vol. 1. Bergen, Norway, 1964, pp. 2–5.

[21] A. Babarit and G. Delhommeau, "Theoretical and numerical aspects of the open source bem solver nemoh," in *Proc. EWTEC*, 2015.

[22] R. Taghipour, T. Perez, and T. Moan, "Hybrid frequency–time domain models for dynamic response analysis of marine structures," *Ocean Eng.*, vol. 35, no. 7, pp. 685–705, 2008.

[23] T. Perez and T. I. Fossen, "A matlab toolbox for parametric identification of radiation-force models of ships and offshore structures," *Modeling, Identification and Control*, vol. 30, no. 1, p. 1, 2009.

[24] Z. Yu and J. Falnes, "State-space modelling of a vertical cylinder in heave," *Appl. Ocean Res.*, vol. 17, no. 5, pp. 265–275, 1995.

[25] E. Kristiansen, Å. Hjulstad, and O. Egeland, "State-space representation of radiation forces in time-domain vessel models," *Ocean Eng.*, vol. 32, no. 17, pp. 2195–2216, 2005.

[26] J. V. Wehausen, "Causality and the radiation condition," *J. Eng. Math.*, vol. 26, no. 1, pp. 153–158, 1992.

[27] S.-Y. Kung, "A new identification and model reduction algorithm via singular value decomposition," in *Proc. Asilomar Conf. on circuits, systems and computers*, 1978, pp. 705–714.

[28] M. Safonov and R. Chiang, "A schur method for balanced model reduction," in *Proc. ACC*. IEEE, 1988, pp. 1036–1040.

[29] J. V. Ringwood, G. Bacelli, and F. Fusco, "Energy-maximizing control of wave-energy converters: the development of control system technology to optimize their operation," *IEEE Contr. Syst. Mag.*, vol. 34, no. 5, pp. 30–55, 2014.

[30] B. Armstrong-Hélouvry, P. Dupont, and C. C. De Wit, "A survey of models, analysis tools and compensation methods for the control of machines with friction," *Automatica*, vol. 30, no. 7, pp. 1083–1138, 1994.

[31] B. Armstrong, "Friction: Experimental determination, modeling and compensation," in *Proc. IEEE Int. Conf. Robot. Autom.* IEEE, 1988, pp. 1422–1427.

[32] L. Marton and B. Lantos, "Modeling, identification, and compensation of stick-slip friction," *IEEE Trans. Ind. Electron.*, vol. 54, no. 1, pp. 511–521, 2007.

Ron Patton was born in Peru in 1949. He graduated at Sheffield University with BEng, MEng and PhD degrees in Electrical & Electronic Engineering and Control Systems, in 1971, 1974, and 1980, respectively. He currently holds the Chair in Control & Intelligent Systems Engineering at Hull University. He has made a substantial contribution to the field of modelling and design of robust methods for Fault Detection and Isolation (FDI) and Fault tolerant Control (FTC) in dynamic systems as author of 348 papers, including 128 journal papers and 6 books. His research interests are: Robust, multiple-model and de-centralized control strategies for FTC systems and he has a growing interest in FTC methods for renewable energy. He is Life Fellow of IEEE, Senior Member of AIAA and Fellow of the Institute of Measurement and Control.

Siya Jin received her B.Eng., M.Eng. degrees in Aeronautics School from the Northwestern Polytechnical University, Xian, P.R. China, in 2012 and 2015, respectively. She began her Ph.D. in Control & Intelligent Systems Engineering Research Group, University of Hull (UoH), Hull, UK, since 09/2015 sponsored by China Scholarship Council (CSC) and UoH joint scholarships. Her current work focuses on numerical simulations and overall mathematical model development for wave energy convertors.

James Gilbert completed a bachelors degree in control and robotics at the University of Hull in 1986 and proceeded to complete a PhD in Non-linear control of a robot in 1989 at the same institution. Since 1989 he has been a Lecturer, Senior Lecturer and Professor in Engineering at the University of Hull. His research has focused on non-linear control, instrumentation and energy harvesting systems.

Dan Parsons is a Professor in Process Sedimentology at the University of Hull, the Director of the University Research Institute on Energy & Environment. He completed his PhD at the University of Sheffield in 2004 and worked on Post-Doctoral post at the University of Leeds. Dan spent a year at the University of Illinois, USA, before returning to Leeds in 2010. In 2011 Dan moved to the University of Hull, where he is actively researching in several areas related to fluvial, estuarine, coastal and deep marine environments, both looking into the impact of climate change of these sensitive systems and also using information gleaned on modern systems to aid interpretations of the geological record.

Bingyong Guo graduated at Northwestern Polytechnical University with BEng and MSc degrees in Information Countermeasure Technology and Underwater Acoustics, in 2010 and 2013, respectively. He is a current PhD student in Electronic Engineering in the University of Hull. Ongoing research interests lies in the numerical modelling, experimental verification and optimal control system design of wave energy conversion devices.